Journal of Alloys and Compounds 509 (2011) 8008–8012

Contents lists available at ScienceDirect

Journal of Alloys and Compounds

journal homepage: www.elsevier.com/locate/jallcom

Hydrothermal synthesis and photoluminescence of Ce^{3+} and Tb^{3+} doped $La_2Sn_2O_7$ nanocrystals

Jinyu Yang[a,b,*], Yuchang Su[b], Haibin Li[c], Xueying Liu[b], Zhuo Chen[a]

[a] School of Chemistry and Materials Science, Guizhou Normal University, Guiyang 550001, China
[b] School of Materials Science and Engineering, Central South University, Changsha 410083, China
[c] School of Physics and Electronic Science, Changsha University of Science & Technology, Changsha 410083, China

ARTICLE INFO

Article history:
Received 13 September 2010
Received in revised form 22 May 2011
Accepted 23 May 2011
Available online 30 May 2011

Keywords:
Phosphers
Chemical synthesis
Optical properties

ABSTRACT

Phase-pure Ce-/Tb-doped and co-doped lanthanum stannates ($La_2Sn_2O_7$) nanocrystals were synthesized by a co-precipitation process combined with hydrothermal techniques without any further heat treatment. The crystal structure, particle size, morphologies, and photoluminescence properties of the as-synthesized products were investigated by X-ray powder diffraction (XRD), transmission electron microscopy (TEM), and photoluminescence spectroscopy (PL). The as-prepared samples were single-phase cubic pyrochlore-type nanocrystals with a typical size of 10–20 nm. PL spectra showed a dominating green-emitting line around 544 nm attributing to $^5D_4$–$^7F_5$ magnetic dipole transition for Tb^{3+} doped and Ce^{3+}/Tb^{3+} co-doped $La_2Sn_2O_7$ nanocrystals. Meanwhile, the concentration quenching phenomenon was observed in both $La_{2-x}Tb_xSn_2O_7$ and $La_{1.82-x}Ce_xTb_{0.18}Sn_2O_7$ nanocrystals. Furthermore, an interesting enhancement of the energy transfer induced green emission was observed in the as-synthesized $La_{1.82-x}Ce_xTb_{0.18}Sn_2O_7$ nanocrystals.

1. Introduction

Rare earth pyrochlore-type complex oxides [1,2] are of considerable importance for a wide variety of applications, such as hosts for luminescence centers [3], high temperature pigments [4], catalysts [5], and ionic conductors [6]. Pyrochlore-type lanthanum stannates have attracted enormous interest recently due to their excellent chemical and thermal stability, and ability to host rare earth ions in their crystal lattice, especially in the octahedrally coordinated site. Lanthanum compounds have been widely used as host materials for rare earth doped solid state lasers and phosphors [7–9]. It is expected that pyrochlore-type lanthanum stannate will be a promising host material for phosphors. Rare earth doped pyrochlore-type lanthanum stannate has been proven to be phosphate materials for promising applications in photonic devices [10].

Terbium ions are the most important green-emitting luminescent activators for several phosphors [11–13] because it has a sharp emission around 544 nm with high intensity, which is close to the theoretical optimum wavelength for the green component of three primary color centers. Ce^{3+} is also a widely used luminescence activator in optical materials and its properties are well known. Ce^{3+}-activated phosphors show a broad band emission at short wavelength under excitation of VUV and UV light in most host matrixes [14–16], which are useful for displaying, planography, and optical data recording.

Many studies concerning the emission and excitation properties of Tb^{3+} and Ce^{3+} co-activated systems with different hosts have been published [17,18]. However, to the best of our knowledge, few reports have been made regarding the luminescence properties of $La_2Sn_2O_7$ nanoparticles doped and co-doped with Ce^{3+}, Tb^{3+} ions.

In this study, a co-precipitation process combined with hydrothermal techniques was employed to synthesize $La_{1.94}Ce_{0.06}Sn_2O_7$, $La_{2-x}Tb_xSn_2O_7$, and $La_{1.82-x}Ce_xTb_{0.18}Sn_2O_7$ nanoparticles phosphors. The structural properties and morphologies of the as-synthesized nanocrystals were investigated. The photoluminescence properties of the resulting nanocrystals were also studied, and an interesting enhancement of the energy transfer induced green emission was observed in $La_{1.82-x}Ce_xTb_{0.18}Sn_2O_7$ nanocrystals.

2. Material and methods

All the reagents in this study were analytical reagents and used as received without further purification. Deionized water was used throughout. In a representative synthesis route, stoichiometric amounts of high-purity solid oxides of lanthanum, terbium and cerium were dissolved in concentrated nitric acid. The required amount of $SnCl_4{\cdot}5H_2O$ was added by keeping the molar ratio of lanthanon to tin as 1:1. The solution was thoroughly mixed for 1 h and added to the solution of ammonia under

* Corresponding author at: School of Chemistry and Materials Science, Guizhou Normal University, Guiyang 550001, China. Tel.: +86 851 6702134; fax: +86 851 6702134.
E-mail address: jinyuyang@gmail.com (J. Yang).

0925-8388/$ – see front matter © 2011 Elsevier B.V. All rights reserved.
doi:10.1016/j.jallcom.2011.05.082

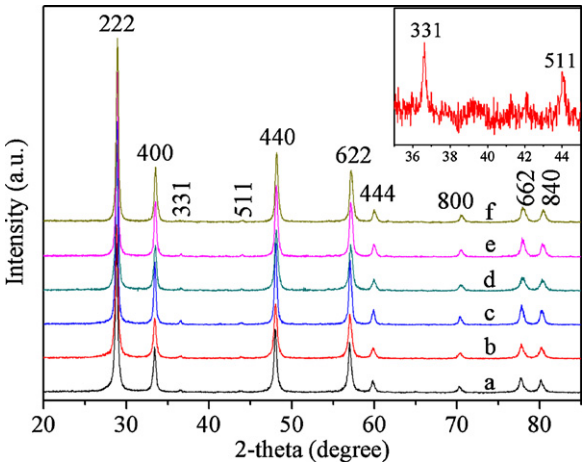

Fig. 1. XRD patterns of the as-synthesized $La_{2-x}Tb_xSn_2O_7$ nanocrystals: (a) $x = 0.02$; (b) $x = 0.06$; (c) $x = 0.10$; (d) $x = 0.14$; (e) $x = 0.18$; (f) $x = 0.22$. A representative zoomed 2θ range (35–45°) of the XRD patterns for $La_{1.94}Tb_{0.06}Sn_2O_7$ sample is shown as an inset.

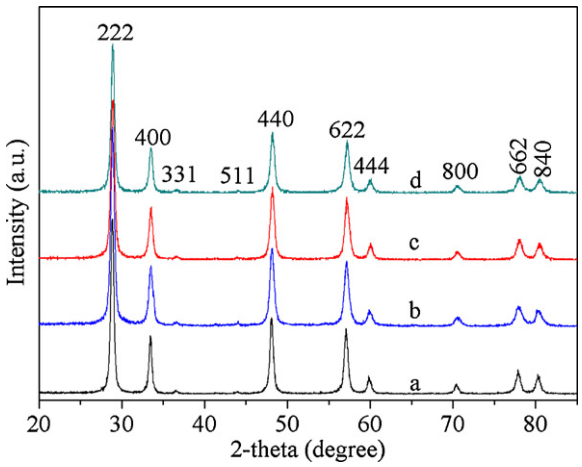

Fig. 2. XRD patterns of the as-synthesized nanocrystals: (a) $La_{1.94}Ce_{0.06}Sn_2O_7$; (b) $La_{1.80}Ce_{0.02}Tb_{0.18}Sn_2O_7$; (c) $La_{1.76}Ce_{0.06}Tb_{0.18}Sn_2O_7$; (d) $La_{1.72}Ce_{0.10}Tb_{0.18}Sn_2O_7$.

continuous stirring at room temperature. Then, the pH of the above solution was adjusted to 12 through the addition of NaOH solution (4 M) and the volume was tailored to 64 ml as well while stirring vigorously on a magnetic stirrer [19]. The solution was vigorously stirred for 1 h before 1.0 g ascorbic acid was added to it. Subsequently, the resulting suspension was transferred into a Teflon-lined stainless steel autoclave (80 ml capacity). The autoclave was maintained at 180 °C for 24 h and cooled naturally to ambient temperature. The precipitates were filtered and washed with deionized water and absolute ethanol several times to remove undesirable ions such as Na^+ and NO_3^-. The precipitates were dried at 100 °C for 4 h in air.

Crystalline phase was identified by X-ray diffraction (XRD) using a Rigaku D/Max 2500 powder diffractometer with Cu Kα radiation (λ = 1.5406 Å). XRD patterns were recorded from 20° to 85° (2θ) with a scan rate of 8°/min. The morphologies of the product particles were observed by transmission electron microscopy (TEM, Philips Tecnai 20 G2 S-TWIN) under an acceleration voltage of 200 kV. The photoluminescence (PL) spectra were measured with a Hitachi F-2500 fluorescence spectrometer at room temperature.

3. Results and discussion

Fig. 1 shows the X-ray diffractions of the as-synthesized $La_{2-x}Tb_xSn_2O_7$ with different Tb-doping contents. As presented in Fig. 1, all the diffraction lines in each pattern can be indexed well to the reference pattern (JCPDS 73-1686). It is well known that four main peaks (2 2 2), (4 0 0), (4 4 0) and (6 2 2) are characteristic of pyrochlore structure. Although similar diffractions were also observed in the defect fluorite structure [20], the reflections from the crystallographic planes (3 3 1) and (5 1 1) of the pyrochlore structure are also found in the patterns. We can confirm that the as-prepared samples possess pyrochlore type structure [21]. A representative zoomed XRD pattern with the 2θ range, ranging from 35° to 45°, was shown as an inset in Fig. 1. Two weak peaks corresponding to (3 3 1) and (5 1 1) peaks could be observed. The results indicated that all samples had a single cubic pyrochlore structure of $La_2Sn_2O_7$ with the space group of *Fd*-3*m* (No. 227). Using Scherrer's equation [22], the crystallite sizes of the samples were calculated from the peak half-width of (2 2 2) peak and were found to be in the range of 10–20 nm. It was worth noting that the diffraction peaks of the samples shifted toward a higher diffraction angle as a result of increasing Tb doping content, indicating that the lattice parameters had decreased due to the differences in ionic radius between La^{3+} (1.06 Å) and Tb^{3+} (0.923 Å) [23], which in according to Vegards's law [24]. This implied that the $La_{2-x}Tb_xSn_2O_7$ products were not simple mixtures of $La_2Sn_2O_7$ and $Tb_2Sn_2O_7$, but homogeneous phase with a cubic pyrochlore structure. That is to say, a small quantity of doped Tb ions had a negligible effect on the crystallographic structures of $La_2Sn_2O_7$.

The XRD patterns of the as-synthesized $La_{1.94}Ce_{0.06}Sn_2O_7$ and $La_{1.82-x}Ce_xTb_{0.18}Sn_2O_7$ samples with different Ce-doping amount were shown in Fig. 2. All the diffraction peaks in the XRD patterns can be assigned to the pyrochlore phase of lanthanum stannate (JCPDS 73-1686). The calculated crystallite sizes of the samples were about 12–19 nm. In Fig. 2, it could also be observed the phenomenon that those XRD peaks slightly shifted to a high degree with the increase of Ce-doping content, similarly as in Fig. 1.

Morphologies of the samples were examined by TEM at room temperature. Representative TEM micrographs of the as-synthesized Ce-/Tb-doped and co-doped $La_2Sn_2O_7$ nanocrystals are shown in Fig. 3(A)–(C), respectively. The images show a homogeneous nanostructure and uniform particles with sizes of 10–20 nm. The sizes of the crystallites were basically consistent with those determined from the XRD patterns. The images clearly display that the nanocrystals commonly occur as hard agglomerates, which is the common character of hydrothermally synthesized $Ln_2Sn_2O_7$ powders [25,26]. In addition, TEM images of the other Ce-/Tb-doped and co-doped $La_2Sn_2O_7$ nanocrystals were similar to those of Fig. 3(A)–(C).

The excitation and emission spectrum of $La_{1.94}Ce_{0.06}Sn_2O_7$ nanocrystals were shown in Fig. 4(A) and (B), respectively. The excitation spectrum of the $La_{1.94}Ce_{0.06}Sn_2O_7$ sample obtained by monitoring the emission band at 377 nm at room temperature, as shown in Fig. 4(A), showed an obvious band around 332.5 nm, attributing to the $^2F_{5/2}$–^2D_J ($J = 5/2, 3/2$) transitions of Ce^{3+} ions. These transitions are parity allowed and have large oscillator strength. However, it is difficult for us to observe the crystal-field splitting of Ce^{3+} 5*d* levels due to the experimental limitations. In consequence, the emission in $La_{1.94}Ce_{0.06}Sn_2O_7$ is efficiently excited by direct excitation of the dopant ions. Under excitation at 332.5 nm, the emission spectrum of the as-synthesized $La_{1.94}Ce_{0.06}Sn_2O_7$ nanocrystals, in Fig. 4(B), consisted of two bands located at 352 nm and 377 nm, corresponding to the $^2D_{3/2}$–^2F_J ($J = 7/2, 5/2$) transitions, respectively. The energy difference between 352 and 377 nm peaks was 1884 cm^{-1}, consistent with the usual ground state splitting of Ce^{3+} in most Ce^{3+} activated phosphors [14].

The excitation and emission spectra were illustrated in Fig. 5(A) and (B) for the as-synthesized $La_{2-x}Tb_xSn_2O_7$ nanocrystals with different Tb-doping contents. The excitation spectra obtained by monitoring the green emission transition at 543 nm revealed a group of excitation bands in the wavelength region from 300 to 500 nm, which correspond to the f–f transitions of the 4f electronic shell of Tb^{3+} ions. These bands could be assigned to the relevant

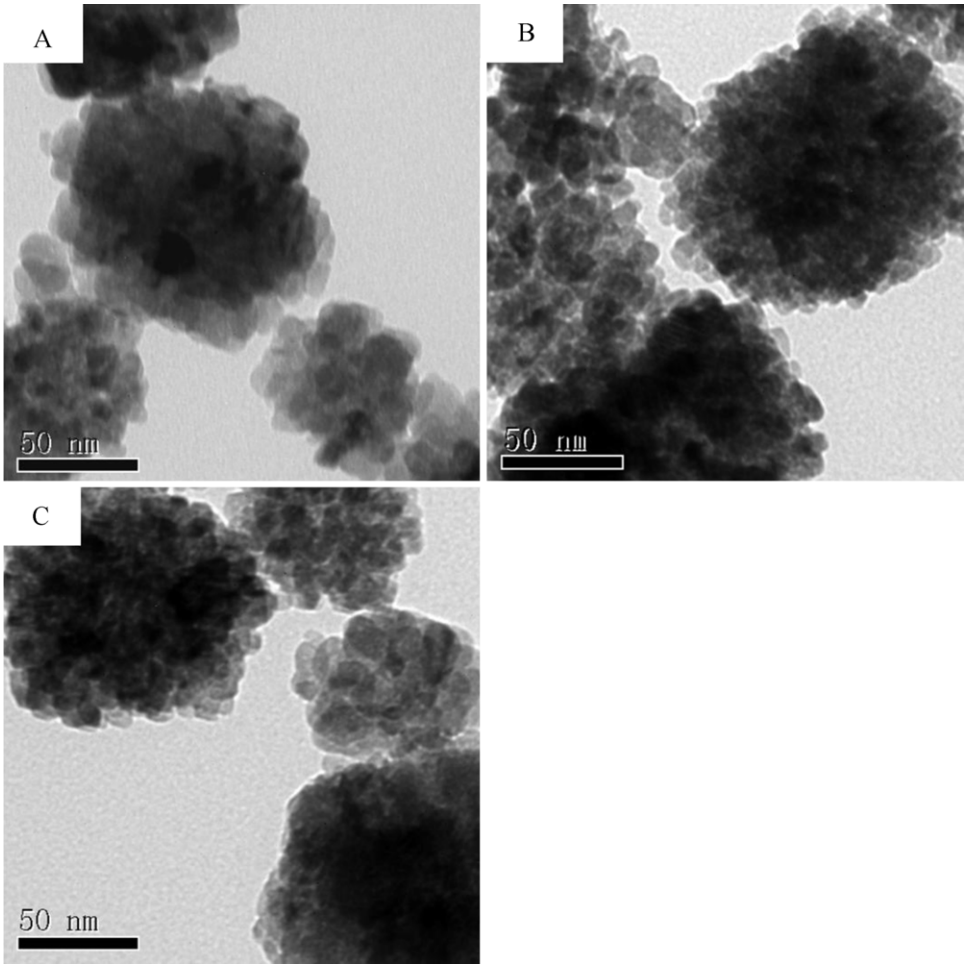

Fig. 3. TEM images of the representative doped $La_2Sn_2O_7$ nanocrystals: (a) $La_{1.94}Ce_{0.06}Sn_2O_7$; (b) $La_{1.86}Tb_{0.14}Sn_2O_7$; (c) $La_{1.76}Ce_{0.06}Tb_{0.18}Sn_2O_7$.

transitions from the ground state ($^7F_6$) to the higher energy levels such as $^5H_6$ (304 nm), $^5D_0$ (319 nm), $^5D_2$ (359 nm), $^5D_3$ (379 nm), and $^5D_4$ (488.5 nm) [27]. A weak peak was also observed at 284 nm, which was ascribed to the spin-forbidden (high-spin) $4f^8$–$4f^7 5d^1$ transition of Tb^{3+}. The strongest excitation peak located at 379 nm is in agreement with a previous report from Zhang et al. [17]. The emission spectrum of $La_{1.94}Ce_{0.06}Sn_2O_7$ and the excitation spectra of $La_{2-x}Tb_xSn_2O_7$ have revealed that there was a significant spectral overlap between the emission band of Ce^{3+} and Tb^{3+} excitation band. Therefore, the effective resonance type energy transfer from Ce^{3+} to Tb^{3+} is expected.

The emission spectra of Tb-activated phosphor measured at 379 nm were shown in Fig. 5(B). Under the excitation of 379 nm, each sample exhibited a similar green luminescence. The strongest emission peak located at 543 nm was ascribed to the magnetic

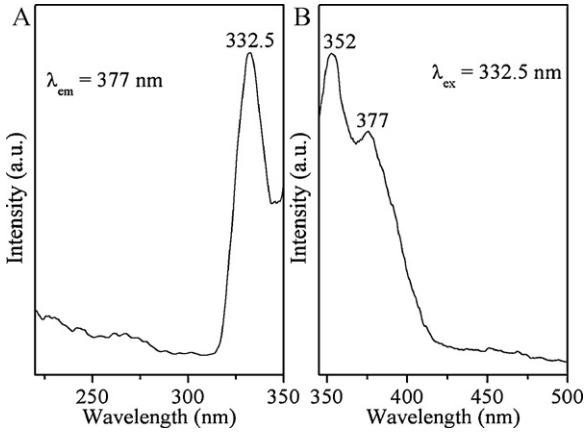

Fig. 4. (A) Excitation spectrum of the as-synthesized $La_{1.94}Ce_{0.06}Sn_2O_7$ nanocrystals at λ_{em} = 377 nm; (B) emission spectrum of $La_{1.94}Ce_{0.06}Sn_2O_7$ sample at λ_{ex} = 332.5 nm.

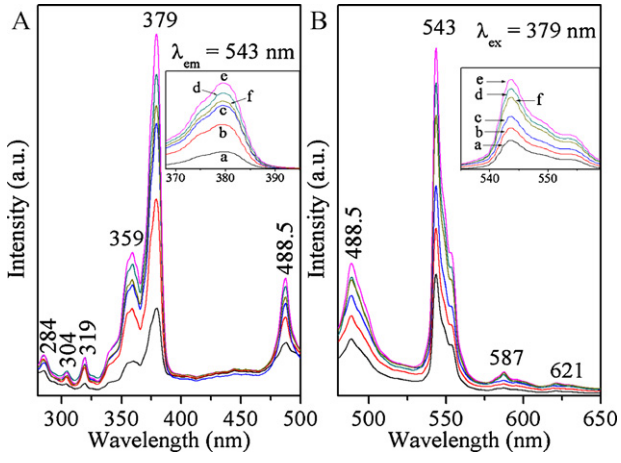

Fig. 5. (A) The excitation spectra and (B) emission spectra of the as-synthesized $La_{2-x}Tb_xSn_2O_7$ nanocrystals: (a) x = 0.02; (b) x = 0.06; (c) x = 0.10; (d) x = 0.14; (e) x = 0.18; (f) x = 0.22.

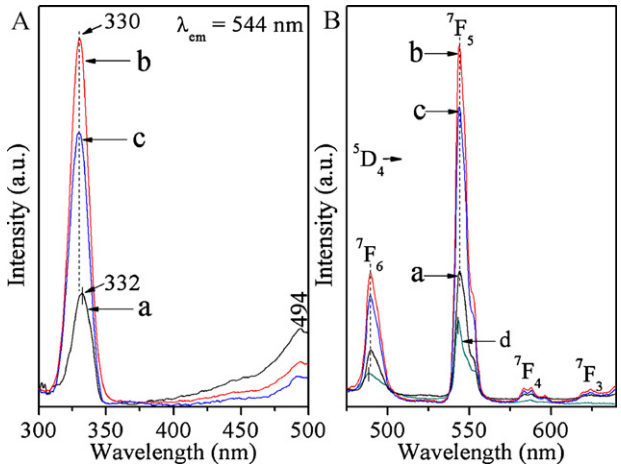

Fig. 6. (A) The excitation spectra of the as-synthesized $La_{1.92-x}Ce_xTb_{0.18}Sn_2O_7$ nanocrystals: (a) $x = 0.02$; (b) $x = 0.06$; (c) $x = 0.10$; (B) the emission spectra of the as-synthesized nanocrystals: (a) $La_{1.80}Ce_{0.02}Tb_{0.18}Sn_2O_7$ ($\lambda_{ex} = 330$ nm); (b) $La_{1.76}Ce_{0.06}Tb_{0.18}Sn_2O_7$ ($\lambda_{ex} = 330$ nm); (c) $La_{1.72}Ce_{0.10}Tb_{0.18}Sn_2O_7$ ($\lambda_{ex} = 330$ nm); (d) $La_{1.82}Tb_{0.18}Sn_2O_7$ ($\lambda_{ex} = 379$ nm).

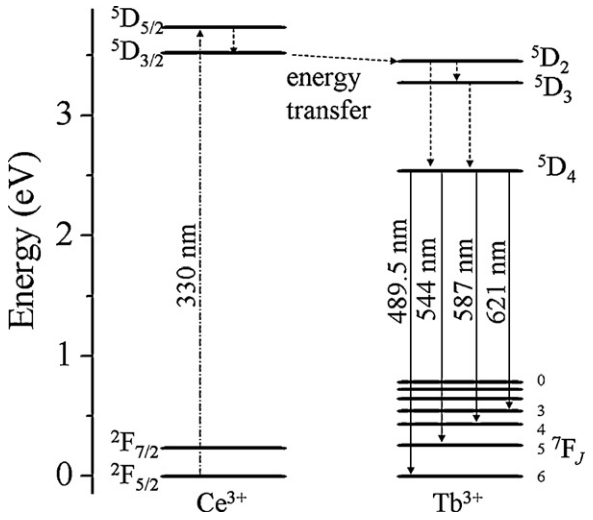

Fig. 7. Energy-level diagram of $(La_{1.82-x}Ce_xTb_{0.18})Sn_2O_7$ ($x > 0$) nanocrystals with radiative transitions and energy transfer processes. Dashed-doted arrow: excitation; dashed arrows: non-radiative decay; solid arrows: radiative decay.

dipole $^5D_4$–$^7F_5$ transition of Tb^{3+}. The other peaks at 488.5, 587 and 621 nm were corresponded to $^5D_4$–$^7F_6$, $^5D_4$–$^7F_4$, and $^5D_4$–$^7F_3$ transitions of Tb^{3+}, respectively.

The variation of the luminescent intensity with Tb^{-}doping content could also be seen in Fig. 5. The $^5D_4$–$^7F_5$ transition intensity increased initially, reached a maximum value at $x = 0.18$, and then decreased with the increase of Tb-doping concentration, indicating that the concentration quenching to occur if the activator concentration increases above the critical concentration, i.e. $x > 0.18$. As the Tb^{3+} concentration increases, the distance between adjacent Tb^{3+} ions decrease, facilitating the energy transfer between neighboring Tb^{3+} ions. The concentration quenching effect was attributed to the possible non-radiative energy transfer between neighboring Tb^{3+} ions, which increase the mobility of the excited states within the host matrix and, therefore, increase the probability of non-radiative de-excitation via traps. The optimum concentration of Tb^{3+} is different from what others reported because it is a variable depending on the excitation source and the host matrix [12,28].

The luminescence characteristics of $(La_{1.82-x}Ce_xTb_{0.18})Sn_2O_7$ nanocrystals with different Ce-doping contents were explored. The excitation spectra of $(La_{1.82-x}Ce_xTb_{0.18})Sn_2O_7$ nanocrystals were obtained upon detection at 544 nm (Fig. 6(A)). The excitation spectra showed a band at around 330 nm along with a weak band at 494 nm, which were assigned to the $^2F_{5/2}$–^2D_J ($J = 5/2, 3/2$) transitions of Ce^{3+} and the $^7F_6$–$^5D_4$ transition of Tb^{3+} [29], respectively, and no other obvious excitation peaks could be observed. As the Ce-doping content increased from 0.02 to 0.10, the band of the $^2F_{5/2}$–^2D_J ($J = 5/2, 3/2$) transitions exhibited a blue shift from 332 nm to 330 nm. The intensity first increased and reached a maximum at $x = 0.06$ then decreased. The blue shift phenomenon indicated that the lowest 5d level had a shift to lower energy level. It was reported that the unit cell affected the crystal field around Ce^{3+}, and led to blue shift of spectra [30]. The lattice constants decreased with increasing Ce-doping constant, as the analysis of XRD patterns revealed (Fig. 2). Therefore, the blue shift of peak located around 330 nm was resulted from the change of crystal field around Ce^{3+} ions.

Fig. 6(B) showed the emission spectra of the $(La_{1.82}Tb_{0.18})Sn_2O_7$ and $(La_{1.82-x}Ce_xTb_{0.18})Sn_2O_7$ phosphors with different dopant contents. The excitation wavelength was 330 nm for $(La_{1.82-x}Ce_xTb_{0.18})Sn_2O_7$ ($x > 0$) phosphors and 379 nm for $(La_{1.82}Tb_{0.18})Sn_2O_7$ sample. As shown in Fig. 6(B), the emission spectra were similar in shape and differ in the band intensities. That emission spectra consisted of four main bands between 450 and 640 nm, which corresponded to the $^5D_4$–^7F_J ($J = 6, 5, 4, 3$) transitions of Tb^{3+} activators. It was remarkable that the co-doped samples exhibited an enhancement of Tb^{3+} overall emission compared with the $(La_{1.82}Tb_{0.18})Sn_2O_7$ sample. Especially, the $(La_{1.74}Ce_{0.06}Tb_{0.18})Sn_2O_7$ had the strongest emission intensity and the emission intensity around 544 nm was 3.1 times higher than that of $(La_{1.82}Tb_{0.18})Sn_2O_7$, although the Tb content was the same for both. Moreover, those $^5D_4$–^7F_J ($J = 3$, 4, 5 and 6) transitions of those co-doped samples showed a slight red shift as compared with that of Tb^{3+} doped samples, which was probably attributed to the distortion of dodecahedral symmetry around Tb^{3+} ions brought about by Ce^{3+} substitution and subsequent lowering of 5d energy level due to the large covalency. In addition, for the $(La_{1.82-x}Ce_xTb_{0.18})Sn_2O_7$ samples, the concentration quenching could also be observed at $x = 0.10$. In a word, in the co-doped $(La_{1.82-x}Ce_xTb_{0.18})Sn_2O_7$ system, the typical Tb^{3+} emission originated from the excitation band of Ce^{3+} at 330 nm and the photoluminescence intensity depended on the Ce^{3+} concentration were strong evidences that the efficient energy transfer from Ce^{3+} to Tb^{3+} occurred. The phenomenon of energy transfer from Ce^{3+} to Tb^{3+} had been already reported [31–33].

The energy transfer process from Ce^{3+} to Tb^{3+} was schematically depicted in Fig. 7. First, the UV photons (at 330 nm) are absorbed by Ce^{3+} ions, resulting in the Ce^{3+} ions excited to the $^5D_{5/2}$ level. Then, excited Ce^{3+} ions in the $^5D_{5/2}$ level may relax non-radiatively to the first excited level, $^5D_{3/2}$ level. Subsequently, excited Ce^{3+} ions in the first excited level may transfer their energy to nearby ground state of Tb^{3+} ions, thereby exciting them into the $^5D_2$ level, which decay non-radiatively to the $^5D_4$ level followed by radiative decay to various lower levels of $7F_J$ ($J = 3$–6). As a result, the as-synthesized $(La_{1.82-x}Ce_xTb_{0.18})Sn_2O_7$ ($x > 0$) nanocrystals exhibits a strong green PL band centered at around 544 nm under 330 nm light excitation. It was well understood that increasing the concentration of Ce^{3+} ions would enhance the energy transfer rate from the $^5D_{3/2}$ level of Ce^{3+} to the $^5D_2$ level of Tb^{3+}, which would cause the high luminescence intensity of Tb^{3+} ions in the co-doped $La_2Sn_2O_7$ system. Simultaneously, it was expected that increasing the content of Ce^{3+} ions in $(La_{1.82-x}Ce_xTb_{0.18})Sn_2O_7$ ($x > 0$) matrix would increase the probability of forming Ce^{3+}–Ce^{3+} pairs due to the decreasing distance of neighboring Ce^{3+} ions. Those Ce^{3+}–Ce^{3+} pairs play the role of an energy consumer via a cross-relaxation

process [34], which suppresses the energy transfer from Ce^{3+} to Tb^{3+} and the luminescence of Tb^{3+} ions quenching.

4. Conclusions

Phase-pure terbium and cerium doped and co-doped $La_2Sn_2O_7$ nanocrystals have been successfully synthesized by a co-precipitation combined with a hydrothermal process without any further calcination treatment. The characterization of XRD and TEM of samples revealed that the as-synthesized nanocrystals had approximately 10–20 nm diameters. The $La_{1.94}Ce_{0.06}Sn_2O_7$ nanocrystals emitted two bands located at 352 nm and 377 nm, corresponding to $^2D_{3/2}$–^2F_J (J = 7/2, 5/2) transitions. The $La_{2-x}Tb_xSn_2O_7$ nanocrystals emitted a dominating and intense line at 543 nm, attribute to $^5D_4$–$^7F_5$ magnetic dipole transition. Concentration quenching was observed for $La_{2-x}Tb_xSn_2O_7$ nanocrystals. The optimum doped concentration for Tb^{3+} was determined to be 0.18 for x in $La_{2-x}Tb_xSn_2O_7$ phosphors. In the as-synthesized $(La_{1.82-x}Ce_xTb_{0.18})Sn_2O_7$ ($x > 0$) nanocrystals, the Ce^{3+} ions strongly sensitize the luminescence of the Tb^{3+} ions, it is likely that energy transfer from Ce^{3+} to Tb^{3+} occurs. The $(La_{1.74}Ce_{0.06}Tb_{0.18})Sn_2O_7$ sample emitted 3.1 times higher luminescence intensity of $^5D_4$–$^7F_5$ transition than that of $(La_{1.82}Tb_{0.18})Sn_2O_7$ sample. Concentration quenching was also observed in $(La_{1.82-x}Ce_xTb_{0.18})Sn_2O_7$ ($x > 0$) system and the optimum Ce-doped content was 0.06. The results from this study may provide some information to develop new phosphor materials and $(La_{1.82-x}Ce_xTb_{0.18})Sn_2O_7$ ($x > 0$) is a promising green-emitting phosphor for applications in lamps and displays.

Acknowledgements

The authors acknowledge the financial support from Guangxi Natural Science Foundation (no. 2010GXNSFB013008), the Doctors Research Foundation of Guizhou Normal University, and the Graduate degree thesis Innovation Foundation of Central South University (no. 2009bsxt001).

References

[1] L.K. Joseph, K.R. Dayas, S. Damodar, B. Krishnan, K. Krishnankutty, V.P.N. Nampoori, R. Radhakrishnan, Photoluminescence studies on rare earth titanates prepared by self-propagating high temperature synthesis method, Spectrochim. Acta, Part A 71 (2008) 1281–1285.
[2] A. Alemi, R.E. Kalan, Preparation and characterization of neodymium tin oxide pyrochlore nanocrystals by the hydrothermal method, Radiat. Eff. Defects Solids 163 (2008) 229–236.
[3] J. Yang, Y. Su, L. Li, Novel tube-like $Y_2Sn_2O_7$:Tb^{3+} crystals: hydrothermal synthesis and photoluminescence properties, Chem. Lett. 39 (2010) 182–183.
[4] F. Matteucci, G. Cruciani, M. Dondi, G. Baldi, A. Barzanti, Crystal structural and optical properties of Cr-doped $Y_2Ti_2O_7$ and $Y_2Sn_2O_7$ pyrochlores, Acta Mater. 55 (2007) 2229–2238.
[5] J. Zeng, H. Wang, Y. Zhang, M. Zhu, H. Yan, Hydrothermal synthesis and photocatalytic properties of pyrochlore $La_2Sn_2O_7$ nanocubes, J. Phys. Chem. C 111 (2007) 11879–11887.
[6] M.R. Diaz-Guillen, K.J. Moreno, J.A. Diaz-Guillen, A.F. Fuentes, K.L. Ngai, J. Garcia-Barriocanal, J. Santamaria, C. Leon, Cation size effects in oxygen ion dynamics of highly disordered pyrochlore-type ionic conductors, Phys. Rev. B 78 (2008) 104304.
[7] D. Mohr, A.S.S. de Camargo, J.F. Schneider, T.B. Queiroz, H. Eckert, E.R. Botero, D. Garcia, J.A. Eiras, Solid state NMR as a new approach for the structural characterization of rare-earth doped lead lanthanum zirconate titanate laser ceramics, Solid State Sci. 10 (2008) 1401–1407.
[8] H.L. Zhu, E. Zhu, H. Yang, L. Wang, D.L. Jin, K.H. Yao, High-brightness $LaPO_4$:Ce^{3+},Tb^{3+} nanophosphors: reductive hydrothermal synthesis and photoluminescent properties, J. Am. Ceram. Soc. 91 (2008) 1682–1685.
[9] G. Liu, X. Duan, H. Li, H. Dong, L. Zhu, Novel polyhedron-like t-$LaVO_4$:Dy^{3+} nanocrystals: hydrothermal synthesis and photoluminescence properties, J. Cryst. Growth 310 (2008) 4689–4696.
[10] A.J. Garcia-Adeva, Band gap atlas for photonic crystals having the symmetry of the kagome and pyrochlore lattices, New J. Phys. 8 (2006) 86–101.
[11] S. Mukherjee, V. Sudarsan, R.K. Vatsa, S.V. Godbole, R.M. Kadam, U.M. Bhatta, A.K. Tyagi, Effect of structure, particle size and relative concentration of Eu^{3+} and Tb^{3+} ions on the luminescence properties of Eu^{3+} co-doped Y_2O_3:Tb nanoparticles, Nanotechnology 19 (2008) 325704.
[12] A Potdevin, G. Chadeyron, D. Boyer, R. Mahiou, Sol-gel elaboration and characterization of YAG:Tb^{3+} powdered phosphors, J. Mater. Sci. 41 (2006) 2201–2209.
[13] S. Mahlik, M. Zalewska, M. Grinberg, A.M. Klonkowski, M. Godlewski, Luminescence kinetics in silica gel doped with Tb^{3+} ions and ZnS:Mn^{2+} nanocrystals, J. Lumin. 128 (2008) 921–923.
[14] H. Lai, A. Bao, Y. Yang, Y. Tao, H. Yang, Y. Zhang, L. Han, UV luminescence property of YPO_4:RE (RE = Ce^{3+}, Tb^{3+}), J. Phys. Chem. C 112 (2008) 282–286.
[15] Z.J. Zhang, J.L. Yuan, C.J. Duan, D.B. Xiong, H.H. Chen, J.T. Zhao, G.B. Zhang, C.S. Shi, Vacuum ultraviolet spectroscopic properties of rare earth (RE = Ce,Tb,Eu,Tm,Sm)-doped hexagonal $KCaGd(PO_4)_2$ phosphate, J. Appl. Phys. 102 (2007) 093514.
[16] A. Potdevin, G. Chadeyron, D. Boyer, R. Mahiou, Sol-gel based YAG:Ce^{3+} powders for applications in LED devices, in: M. Stutzmann (Ed.), Montpellier, Wiley-VCH Verlag Gmbh, France, 2006, pp. 65–69.
[17] Y. Zhang, Z.Z. Xu, C.H. Lu, Y.R. Ni, Optical studies of Tb^{3+} doped boro-alumina-silicate glass, J. Rare Earth 25 (2007) 345–349.
[18] Y.Q. Li, N. Hirosaki, R.J. Xie, T. Takeda, M. Mitomo, Yellow-orange-emitting $CaAlSiN_3$:Ce^{3+} phosphor: structure, photoluminescence, and application in white LEDs, Chem. Mater. 20 (2008) 6704–6714.
[19] J. Yang, Y. Su, X. Liu, Hydrothermal synthesis, characterization and optical properties of $La_2Sn_2O_7$:Eu^{3+} micro-octahedra, Trans. Nonferr. Met. Soc. 21 (2011) 535–543.
[20] S. Esmaeilzadeh, J. Grins, A.K. Larsson, An electron and X-ray powder diffraction study of the defect fluorite structure of $Mn_{0.6}Ta_{0.4}O_{1.65}$, J. Solid State Chem. 145 (1999) 37–49.
[21] A.Y. Zhang, M.K. Lu, Z.S. Yang, G.J. Zhou, Y.Y. Zhou, Systematic research on $RE_2Zr_2O_7$ (RE = La, Nd, Eu and Y) nanocrystals: preparation, structure and photoluminescence characterization, Solid State Sci. 10 (2008) 74–81.
[22] A Patterson, The Scherrer formula for X-ray particle size determination, Phys. Rev. 56 (1939) 978–982.
[23] D.R. Lide, CRC Handbook of Chemistry and Physics, 87th ed., Taylor and Francis, Boca Raton, 2007.
[24] A.R. West, Solid State Chemistry and its Applications, Wiley, New Delhi, 1984.
[25] K.W. Li, T.T. Zhang, H. Wang, H. Yan, Low-temperature synthesis and structure characterization of the serials $Y_{2-\delta}$ $Bi_\delta Sn_2O_7$ ($\delta = 0 - 2.0$) nanocrystals, J. Solid State Chem. 179 (2006) 1029–1034.
[26] H. Cheng, L. Wang, Z. Lu, A general aqueous sol-gel route to $Ln_2Sn_2O_7$ nanocrystals, Nanotechnology 19 (2008) 025706.
[27] J. Yang, C. Zhang, L. Wang, Z. Hou, S. Huang, H. Lian, J. Lin, Hydrothermal synthesis and luminescent properties of $LuBO_3$:Tb^{3+} microflowers, J. Solid State Chem. 181 (2008) 2672–2680.
[28] P. Page, R. Ghildiyal, K.V.R. Murthy, Photoluminescence and thermoluminescence properties of $Sr_3Al_2O_6$:Tb^{3+}, Mater. Res. Bull. 43 (2008) 353–360.
[29] Y.P. Naik, M. Mohapatra, N.D. Dahale, T.K. Seshagiri, V. Natarajan, S.V. Godbole, Synthesis and luminescence investigation of RE^{3+} (Eu^{3+}, Tb^{3+} and Ce^{3+})-doped lithium silicate (Li_2SiO_3), J. Lumin. 129 (2009) 1225–1229.
[30] G.D. Xia, S.M. Zhou, J.J. Zhang, J. Xu, Structural and optical properties of YAG:Ce^{3+} phosphors by sol-gel combustion method, J. Cryst. Growth 279 (2005) 357–362.
[31] H. Yang, Y.S. Kim, Energy transfer-based spectral properties of Tb-, Pr-, or Sm-codoped YAG:Ce nanocrystalline phosphors, J. Lumin. 128 (2008) 1570–1576.
[32] D. Wang, Y.H. Wang, Luminescence properties of $LaPO_4$:Tb^{3+}, Me^{3+} (Me = Gd, Bi, Ce) under VUV excitation, Mater. Res. Bull. 42 (2007) 2163–2169.
[33] R. Turos-Matysiak, W. Gryk, M. Grinberg, Y.S. Lin, R.S. Liu, $Tb^{3+} \rightarrow Ce^{3+}$ energy transfer in Ce^{3+}-doped $Y_{3-x}Tb_xGd_{0.65}Al_5O_{12}$, J. Phys.: Condens. Matter 18 (2006) 10531–10543.
[34] L. Zhu, X. Wang, G. Yu, X. Hou, G. Zhang, J. Sun, X. Liu, D. Xu, Effect of Ce^{3+} doping and calcination on the photoluminescence of ZrO_2 (3% Y_2O_3) fibers, Mater. Res. Bull. 43 (2008) 1032–1037.